Increase in efficiency and reduction in Ca^{2+} dependence of exocytosis during development of mouse inner hair cells

Stuart L. Johnson, Walter Marcotti and Corné J. Kros

School of Life Sciences, University of Sussex, Falmer, Brighton BN1 9QG, UK

Developmental changes in the coupling between Ca^{2+} entry and exocytosis were studied in mouse inner hair cells (IHCs) which, together with the afferent endings, form the primary synapse of the mammalian auditory system. Ca^{2+} currents (I_{Ca}) and changes in membrane capacitance (ΔC_m) were recorded using whole-cell voltage clamp from cells maintained at body temperature, using physiological (1.3 mM) extracellular Ca^{2+}. The magnitudes of both I_{Ca} and ΔC_m increased with maturation from embryonic stages until postnatal day 6 (P6). Subsequently, I_{Ca} gradually declined to a steady level of about −100 pA from P13 while the Ca^{2+}-induced ΔC_m remained relatively constant, indicating a developmental increase in the Ca^{2+} efficiency of exocytosis. Although the size of I_{Ca} changed during development, its activation properties did not, suggesting the presence of a homogeneous population of Ca^{2+} channels in IHCs throughout development. The Ca^{2+} dependence of exocytosis changed with maturation from a fourth power relation in immature cells to an approximately linear relation in mature cells. This change applies to the release of both a readily releasable pool (RRP) and a slower secondary pool of vesicles, implying a common release mechanism for these two kinetically distinct pools that becomes modified during development. The increased Ca^{2+} efficiency and linear Ca^{2+} dependence of mature IHC exocytosis, especially over the physiological range of intracellular Ca^{2+}, could improve the high-fidelity transmission of both brief and long-lasting stimulation. These properties make the mature cell ideally suited for fine intensity discrimination over a wide dynamic range.

(Received 28 August 2004; accepted after revision 17 December 2004; first published online 21 December 2004)
Corresponding author C. J. Kros: School of Life Sciences, University of Sussex, Falmer, Brighton BN1 9QG, UK. Email: c.j.kros@sussex.ac.uk

Inner hair cells (IHCs) are the primary sensory cells of the mature mammalian cochlea, responsible for translating sounds into neuronal signals. Sound-induced bundle deflection depolarizes the IHC and leads to the activation of $Ca_v1.3$ L-type voltage-gated Ca^{2+} channels situated in the cell's basolateral membrane (Platzer *et al.* 2000; Brandt *et al.* 2003; Hafidi & Dulon, 2004). Ca^{2+} entry triggers the fusion of synaptic vesicles to the basolateral membrane and glutamate is released onto afferent terminals (Glowatzki & Fuchs, 2002). Mature IHCs respond to sound stimulation with graded receptor potentials that increase with sound intensity (Russell & Sellick, 1978) from around 12 days after birth (P12). Although immature IHCs do not respond to sound, they fire spontaneous and depolarization-induced Ca^{2+} action potentials (Kros *et al.* 1998; Marcotti *et al.* 2003*a*,*b*), thought to affect the remodelling of synaptic connections that occurs during development (Pujol *et al.* 1998). Synaptic machinery is present in mouse IHCs from birth (Sobkowicz *et al.* 1982) and appears already to be functional at this time (Beutner & Moser, 2001; Marcotti *et al.* 2003*b*). This suggests that action potentials could drive neurotransmitter release onto afferent fibres, which has been indirectly demonstrated from 'bursts' of afferent activity that match the duration and frequency of Ca^{2+} action potentials in P7 rat IHCs (Glowatzki & Fuchs, 2002).

At around the onset of hearing, the synaptic machinery changes from multiple spherical bodies, typical of immature cells, to single flat plate-like ribbons at each active zone (Sobkowicz *et al.* 1982). The change in synaptic architecture and response properties during development may have evolved to ensure that IHCs are optimally configured to respond to different membrane voltage excursions before and after the onset of hearing. In addition to these morphological findings, the onset of functional maturation in the cochlea is also characterized by an increase in the Ca^{2+} efficiency of readily releasable pool (RRP) exocytosis in IHCs (Beutner & Moser, 2001), although these results were obtained using unphysiological

 DOI: 10.1113/jphysiol.2004.074740

recording conditions (room temperature and 10 mM extracellular Ca^{2+}).

In this study we compare directly whole-cell current recordings and membrane capacitance measurements from apical IHCs during development to investigate changes in the properties of their Ca^{2+} currents (I_{Ca}) and synaptic vesicle exocytosis, at body temperature and using a physiological concentration of extracellular Ca^{2+} (1.3 mM; Wangemann & Schacht, 1996). We show that in IHCs the Ca^{2+} efficiency of exocytosis of mainly an identified RRP of vesicles increases during development whereas, in contrast to previous investigations, the Ca^{2+} dependence of both RRP and secondary vesicle pools reduces, which could be consistent with a transition in the synaptic machinery to optimize the mature IHC for auditory transduction. Moreover, the kinetics and size of the RRP and the secondary pool differ from those obtained using high extracellular Ca^{2+}.

Methods

Tissue preparation

Apical-coil IHCs were studied in acutely dissected organs of Corti from Swiss CD-1 mice (Charles Rivers, Margate, UK) ranging from embryonic-day 16.5 (E16.5) up to P20 where the day of birth (P0) corresponds to E19.5. For embryonic experiments only, mice were paired overnight and checked for vaginal plugs the following morning. Assuming ovulation occurs midway through the dark cycle, the midpoint of the light cycle of the day following mating is considered to be E0.5. Mature and neonatal mice were killed by rapid cervical dislocation and embryos by decapitation, in accordance with UK Home Office guidelines. Cochleae were transferred to a microscope chamber and immobilized under nylon mesh. The chamber was continuously perfused with extracellular solution containing (mM): 135 NaCl, 5.8 KCl, 1.3 $CaCl_2$, 0.9 $MgCl_2$, 0.7 NaH_2PO_4, 5.6 D-glucose, 10 Hepes-NaOH, 2 sodium pyruvate. Amino acids and vitamins (Invitrogen, Paisley, UK) for Eagle's MEM were added from concentrates. The pH was 7.5 and the osmolality 308 mmol kg^{-1}. The chamber was mounted on an upright microscope (Olympus, Tokyo, Japan) and cells were observed with Nomarski DIC optics. The position of the cells was recorded as fractional distance along the cochlea starting from the extreme apex. In the immature cochlea, cells were positioned in the apical coil at a fractional distance of between 0.12 and 0.26. Mature cells were positioned between 0.06 and 0.19, corresponding to an approximate frequency range of 0.8–3.0 kHz (using eqn (13) in Ehret, 1975). Access to IHCs was gained using a suction pipette (tip diameter approximately 3–4 μm) filled with extracellular solution to create a small tear in the epithelium around the cells and expose their basolateral membranes. Only cells of a healthy appearance and with well-preserved hair bundles were investigated.

Electrical recording

Current recordings from apical IHCs ($n = 226$), maintained near body temperature (34–37°C) and in 1.3 mM extracellular Ca^{2+}, were obtained using whole-cell patch clamp with an Optopatch amplifier (Cairn Research Ltd, Faversham, UK). Patch electrodes were pulled from soda glass capillaries (Harvard Apparatus Ltd, Edenbridge, UK) and coated with surf wax (Mr Zogs SexWax, Carpinteria, CA, USA) to minimize the fast electrode capacitative transients. The pipette filling solution contained (mM): 140 Cs-glutamate, 3 $MgCl_2$, 5 Na_2ATP, 0.3 Na_2GTP, 1 EGTA-CsOH, 5 Hepes-CsOH (pH 7.3, 290 mmol kg^{-1}). Data were acquired using pClamp software and a Digidata 1320 A (Axon Instruments, CA, USA), filtered at 2.5 kHz or 10 kHz (8-pole Bessel), sampled at 5 kHz or 50 kHz, respectively, and stored on computer. Offline data analysis was performed using Clampfit (Axon Instruments) and Origin software (OriginLab, Northampton, MA, USA). Current recordings were corrected for linear leak conductance (g_{leak}) measured near −81 mV (1.6 ± 0.1 nS, $n = 204$). Since the leak conductance was not measured for some of the postnatal cells (P0–P6) in Fig. 1, averaged values from age-matched cells were used instead in these cases. Membrane potentials were corrected for residual series resistance (R_s, 6.0 ± 0.1 MΩ, $n = 226$) and a liquid junction potential of −11 mV, measured between electrode and bath solutions. The voltage-clamp time constant was 48.3 ± 0.2 μs ($n = 226$).

Membrane capacitance measurement

Real-time change in membrane capacitance (ΔC_m) was measured using the track-in circuitry of the Optopatch as previously described (Johnson *et al.* 2002). To enable the track-in circuitry to operate, a 2.5 kHz sine wave (amplitude 18.5 mV) was applied to IHCs from a holding potential of either −71 mV (Fig. 1) or −81 mV (Figs 2, 4, 5 and 6) using the internal oscillator of the Optopatch. The sine wave was small enough not to activate any significant membrane current since accurate membrane capacitance calculation requires a high and constant membrane resistance (R_m). The command sine wave was interrupted for the duration of the voltage step, or action potential waveform, so inward currents could be recorded. The capacitance signal from the Optopatch was amplified (×50), 2-pole filtered at 150 Hz with additional 8-pole Bessel filtering at 250 Hz, and sampled at 5 kHz. We allowed approximately 5–10 s per stimulus for vesicle pool replenishment. When multiple step protocols were used

(Fig. 2*A* and Fig. 4*A*) the prestimulus C_m baseline for consecutive steps was set to zero during offline analysis. Changes in membrane capacitance were measured by averaging the C_m trace over a 300 ms period following the voltage step when the prestimulus baseline had been set to zero. Due to the apparent partial C_m recovery immediately after the voltage step, seen in some recordings (Fig. 2*A*), ΔC_m was measured 50 ms after the end of the voltage step. This small decline is likely to be caused by the I_{Ca} tail currents, which significantly reduce R_m. Post-stimulus C_m recovery (endocytosis) was not observed in recordings of up to 2.5 s using 1.3 mM extracellular Ca^{2+} or up to 0.6 s using higher Ca^{2+} concentrations (the longest durations used). Although we allowed 5–10 s in between consecutive steps, no clear evidence for endocytosis was found. This could be explained by the loss of important elements of the endocytotic machinery due to the whole-cell configuration (Parsons *et al.* 1994). This does, however, give us a more accurate representation of the vesicle pool size and Ca^{2+} dependence of exocytosis since the ΔC_m responses are not reduced by endocytosis.

An action potential waveform recorded from a spontaneously active apical-coil P3 IHC under current clamp conditions at 37°C was used as a protocol in Fig. 1. During the spike protocol the changing membrane potential would introduce a capacitative current component that may affect the peak of the recorded currents. However, capacitance compensation was applied at the start of every recording and the track-in circuitry of the Optopatch keeps the membrane capacitance accurately compensated while the sine wave is active. When the sine wave is interrupted, during the spike or voltage step, the compensation remains at the prestimulus value. Therefore, any contamination of the ionic currents by the capacitative current would be minimal. In order to express ΔC_m values as a number of vesicles we used a conversion factor of 37 aF per vesicle, which has previously been calculated from vesicle diameters measured using electron tomography on frog saccular hair cells (Lenzi *et al.* 1999).

Extracellular superfusion

ΔC_m and I_{Ca} were recorded during the superfusion of 30 mM TEA (Fluka, Gillingham, UK), which was a constant in all experiments in order to block most IHC K^+ currents. When I_{Ca} was studied in isolation (Fig. 3), immature IHCs were additionally superfused with 300 nM tetrodotoxin (TTX, Sigma, Gillingham, UK) to block the Na^+ current (Marcotti *et al.* 2003*b*) and mature IHCs with 60 nM iberiotoxin (IbTx, Tocris, Bristol, UK), 10 mM 4-AP (Fluka) and 200 μM linopirdine (RBI, Natick, MA, USA) to block $I_{K,f}$, $I_{K,s}$ and $I_{K,n}$, respectively (Kros *et al.* 1998; Marcotti *et al.* 2003*a*). To test the Ca^{2+} dependence of ΔC_m (Fig. 6), IHCs were superfused with a Ca^{2+}-free solution (containing 0.5 mM EGTA) or solutions containing different Ca^{2+} concentrations (2.5, 5 and 10 mM, in addition to 1.3 mM). One set of experiments was designed to determine whether the inward current induced by the spike protocol was mainly carried by L-type Ca^{2+} channels containing the α1D ($Ca_v1.3$) subunit (Platzer *et al.* 2000). This was achieved by superfusing immature IHCs with an extracellular solution containing 30 μM nifedipine (Sigma). When chemicals or Ca^{2+} that were added to, or removed from, the solution had a concentration >1 mM, NaCl was adjusted to keep the osmolality constant. Solutions were applied via a multibarrelled pipette positioned close to the IHCs.

Statistical analysis

Statistical comparisons of means were made using Student's two-tailed *t* test or, for comparisons of multiple data sets, one-way ANOVA (followed by the Tukey post test). Two-way ANOVA (followed by the Bonferroni post test) was used for Fig. 3*F*. For all statistical tests $P < 0.05$ was used as the criterion for statistical significance and mean values are quoted ± S.E.M. in text and figures.

Results

Neurotransmitter release in response to an action potential

Immature IHCs fire spontaneous Ca^{2+} action potentials (Marcotti *et al.* 2003*b*) from just before birth (E18.5 in apical IHCs), and this activity lasts until the end of the first postnatal week (Marcotti *et al.* 2003*a*). This spontaneous activity could be important for the remodelling of synaptic connections within the organ of Corti before the onset of sound-evoked responses (Shnerson *et al.* 1982; Echteler, 1992; Pujol *et al.* 1998). To influence the development of afferent fibres, Ca^{2+} influx into immature IHCs that is induced by an action potential should be sufficient to trigger exocytosis. The fusion of synaptic vesicles to the cell membrane can be measured as an increase in cell membrane capacitance (ΔC_m) that is generally interpreted as a sign of neurotransmitter release from presynaptic cells (Neher & Marty, 1982; Parsons *et al.* 1994; von Gersdorff *et al.* 1998; Moser & Beutner, 2000).

To test this hypothesis, a spike protocol (see Methods) was applied to IHCs and the resulting current and ΔC_m were recorded. Typical examples of the inward current and ΔC_m from an E17.5 and a P6 IHC are shown in Fig. 1*A* and *B*, respectively. The inward current was mostly I_{Ca} since it was substantially reduced during the superfusion of a Ca^{2+}-free solution (Fig. 1*C* and Marcotti *et al.* 2003*b*)

and nifedipine (Fig. 1*D*), a blocker of L-type Ca^{2+} channels containing the α1D ($Ca_v1.3$) subunit (Engel *et al.* 2002). The amplitude of I_{Ca} was reduced by $82 \pm 1\%$ (P3–P4, $n = 7$) in a Ca^{2+}-free solution and by $63 \pm 6\%$ (P4, $n = 5$) using 30 μM nifedipine. Moreover the Na^+ current, known to be expressed in about 70% of immature IHCs, becomes largely inactivated during the slow depolarization leading up to the spike threshold potential of about -60 mV (Marcotti *et al.* 2003*b*). For this reason, the inward current elicited by an action potential was referred to as I_{Ca}. Consistent with the decrease in the size of I_{Ca} the ΔC_m was reduced (Fig. 1*C* and *D*) by $89 \pm 1\%$ (P3–P4, $n = 7$) in a Ca^{2+}-free solution and by $78 \pm 2\%$ (P4, $n = 5$) using nifedipine.

The peak I_{Ca} corresponds to the peak of the action potential, and the membrane capacitance increase was apparent immediately after the stimulating waveform. Figure 1*E* shows that the amplitudes of the peak inward current and ΔC_m, in response to the spike protocol, increase as a function of development. Both I_{Ca} and ΔC_m data sets in Fig. 1*E* could be approximated with a sigmoidal logistic growth curve:

$$A = A_{min} + \frac{A_{max} - A_{min}}{1 + \exp(-k(t - t_{1/2}))} \quad (1)$$

where A is the amplitude of I_{Ca} or ΔC_m, k a slope factor, and $t_{1/2}$ the age where A is halfway between maximal (A_{max}) and minimal (A_{min}) values. The fits to I_{Ca} and ΔC_m data points in Fig. 1*E* gave values for $t_{1/2}$ and k of P1.6, 1.8 day^{-1} and P1.2, 1.8 day^{-1}, respectively. These results show that the number of synaptic vesicles released is closely related to the development of I_{Ca}. Although small I_{Ca} and ΔC_m responses were observed at E16.5, the small amplitude of I_{Ca} appears not to be sufficient to allow spontaneous action potentials before E18.5, indicating that the synaptic machinery is likely to be functional about two days before the onset of spontaneous activity.

Developmental changes in I_{Ca} and ΔC_m

We used voltage steps to investigate the development of I_{Ca} and ΔC_m from embryonic to mature stages (E16.5–P20). The use of action potential waveforms is not appropriate for mature cells, which respond to sound stimulation with graded receptor potentials, and the steps allowed a more detailed investigation of ΔC_m dynamics by manipulating the stimulus amplitude and duration. Figure 2*A* shows the inward current and ΔC_m recorded from an immature (P6) and a mature (P20) IHC using a series of 100 ms voltage steps from -81 mV to near -11 mV (peak responses). The current recordings are labelled 'I' rather than 'I_{Ca}' since they are likely to be contaminated by the presence of a residual unblocked SK current in immature IHCs and a delayed rectifier K^+ current ($I_{K,s}$) in mature cells (Marcotti *et al.* 2003*a*,*b*). However, the size of the peak inward current is referred to as I_{Ca} since these slowly activating K^+ currents are relatively small at this time point but would become more evident towards the end of the voltage steps and cause the apparent large current inactivation (Fig. 2*A*). When a Na^+ current was present, the inward current was measured at about 1.5 ms from the onset of the voltage step, by which time the Na^+ current is inactivated (see Fig. 6*A* in Marcotti *et al.* 2003*b*). Although the mature IHC responded to the same voltage step with a significantly smaller peak I_{Ca}, the induced ΔC_m reached a value comparable to that seen in the immature cell. The ΔC_m–voltage (ΔC_m–V) and peak I_{Ca}–voltage (I–V) curves for immature ($n = 8$) and mature ($n = 8$) cells were obtained from responses to 100 ms depolarizing voltage steps, in nominal 10 mV increments, from the holding potential of -81 mV to $+49$ mV (Fig. 2*B*). At both stages, I_{Ca} and ΔC_m follow a bell-shaped pattern, but note the narrower voltage range for ΔC_m for immature cells.

Figure 2*C* shows the developmental changes in ΔC_m and peak I_{Ca} following a 100 ms depolarizing voltage step to around -11 mV. I_{Ca} (Fig. 2*C*, lower panel) increased in size ($P < 0.0001$) from E16.5 until P6 and then gradually declined ($P < 0.0001$), reaching a steady-state level of -100 ± 4 pA (P13–P20, $n = 27$) from P13. The average membrane potential that elicited the peak I_{Ca} (i.e. the peak of the I–V curves) was -12.4 ± 0.9 mV ($n = 149$) over the entire age range tested. The size of ΔC_m (Fig. 2*C*, upper panel) did not decline during development as would be expected if ΔC_m were directly linked to the size of I_{Ca} (Fig. 2*C*, lower panel). Early in development, the changes in ΔC_m reflect that of I_{Ca} as ΔC_m also increased significantly ($P < 0.0005$, E16.5-P6). However, ΔC_m did not change significantly after P6 (26.6 ± 1.1 fF, $n = 108$, P6-P20). The average membrane potential that elicited the peak ΔC_m response (peak of the ΔC_m–V curves) was -11.5 ± 0.7 mV ($n = 149$).

The discrepancy between the development of I_{Ca} and ΔC_m from about P6 onwards suggests that capacitance change, and therefore neurotransmitter release, becomes more efficient in mature cells, in the sense that less Ca^{2+} entry is required to elicit the same ΔC_m response. A similar finding has previously been shown in IHCs but only for small I_{Ca} that elicited ΔC_m of up to 5 fF (Beutner & Moser, 2001). The Ca^{2+} efficiency of exocytosis (Fig. 2*D*) was estimated by normalizing ΔC_m to peak I_{Ca} (fF pA^{-1}) and from P11 onwards the $\Delta C_m/I_{Ca}$ ratio significantly increased ($P < 0.05$), showing that the release of neurotransmitter does indeed become more efficient in mature IHCs. Although embryonic IHCs show an apparently larger Ca^{2+} efficiency of exocytosis compared to that of early postnatal cells, the S.E.M. for these small responses was large and the mean values were not significantly different.

I_{Ca} in immature and mature IHCs

The reduction in I_{Ca} amplitude from the beginning of the second postnatal week (Fig. 2*C*) could be caused by a variety of factors such as a reduction in the number of Ca^{2+} channels per IHC, the expression of channel regulatory subunits or the insertion of another type of Ca^{2+} channel into the basolateral membrane in place of that expressed during earlier stages of development. A reduction in the number of Ca^{2+} channels should only affect the current magnitude and not the current kinetics, whereas the appearance of regulatory subunits (Singer *et al.* 1991) or the expression of a new channel type should have a significant effect on the kinetics. Therefore, we investigated whether the biophysical properties of I_{Ca} in immature (P5–P6) and mature

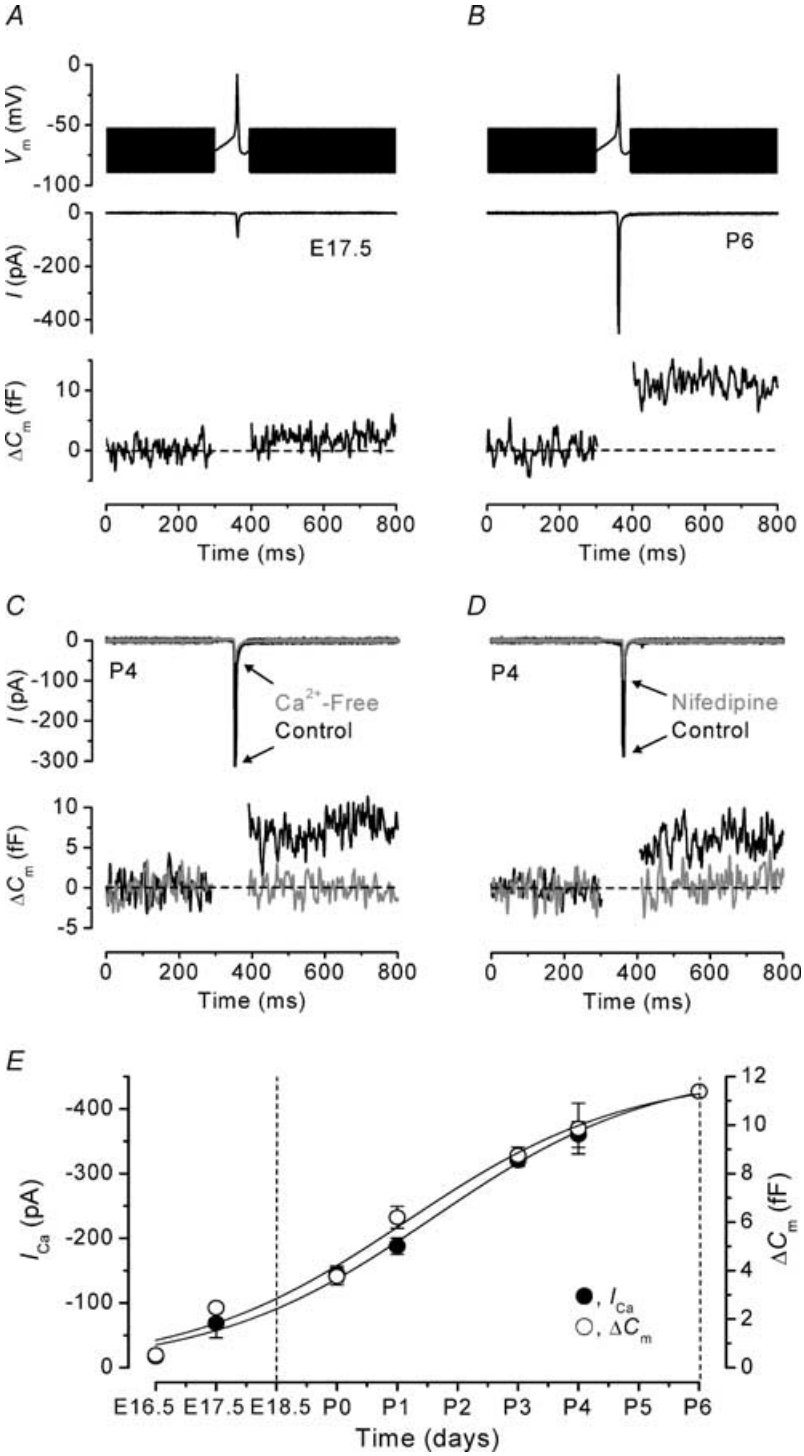

Figure 1. I_{Ca} and ΔC_m responses to a voltage-clamp spike protocol
A and *B*, I_{Ca} and ΔC_m from an E17.5 and a P6 IHC, respectively. Top panels show the command protocol consisting of a sine wave (2.5 kHz) that appears as thick solid lines, which is interrupted for the duration of the spike and applied from a holding potential of −71 mV. Middle panels show the inward current elicited by the spike and lower panels show the corresponding ΔC_m responses. Note that the region during the spike in the lower panels is blanked as the track-in circuitry is not operational. The recordings in *A* and *B* are averages of two and four protocol repetitions, respectively, and the broken horizontal lines represent the zero ΔC_m level (as in subsequent figures). E17.5, C_m 5.3 pF; R_s 7.0 MΩ; g_{leak} 0.8 nS. P6, C_m 8.0 pF; R_s 5.3 MΩ; g_{leak} 2.0 nS. *C*, I_{Ca} (top panel) and ΔC_m (bottom panel) responses to the spike protocol from a P4 IHC in control conditions (black traces) and during the superfusion of a Ca^{2+}-free solution (grey traces). The recordings in control and Ca^{2+}-free conditions are averages of three and two repetitions, respectively. C_m 7.6 pF; R_s 5.1 MΩ; g_{leak} 1.7 nS. *D*, I_{Ca} and ΔC_m elicited by the spike protocol from a P4 IHC in control conditions (black traces) and in the presence of 30 μM nifedipine (grey traces). The recordings in control conditions and during the application of nifedipine are averages of four and nine repetitions, respectively. C_m 7.7 pF; R_s 5.2 MΩ; g_{leak} 1.8 nS. *E*, developmental changes (E16.5–P6) in the amplitudes of peak I_{Ca} (●) and ΔC_m (○) in response to the spike protocol. Solid lines are fits to the I_{Ca} and ΔC_m data points using eqn (1). Numbers of cells are (E16.5–P6) 3, 2, 8, 9, 5, 4, 1. The broken vertical lines at E18.5 and P6 delineate the period during which apical-coil IHCs are capable of firing spontaneous action potentials.

(P18–P20) IHCs are different. To isolate I_{Ca}, IHCs were superfused with specific blockers for the other voltage-gated channels characteristic of the two stages of development (see Methods). Figure 3*A* and *B* show typical examples of I_{Ca} recordings from a P6 and a P18 IHC, respectively. Although the time course of I_{Ca} appears similar in immature and mature cells, I_{Ca} has a smaller amplitude in mature cells consistent with the findings of Fig. 2. The peak I_{Ca} measured at different membrane potentials from immature (P6, $n = 14$) and mature (P18–P20, $n = 21$) IHCs is shown in Fig. 3*C*. Both I–V curves are fits using the following equation:

$$I_{Ca} = \frac{g_{max}(V - V_{rev})}{1 + \exp\left(\frac{V_{1/2} - V}{S}\right)} \quad (2)$$

where V is the membrane potential, V_{rev} the reversal potential, g_{max} the maximum chord conductance, $V_{1/2}$ the membrane potential at which the conductance is half activated and the slope factor (S) describes the voltage sensitivity of activation. The peak I_{Ca}, measured near −11 mV, in immature IHCs (−350 ± 13 pA, $n = 14$) was

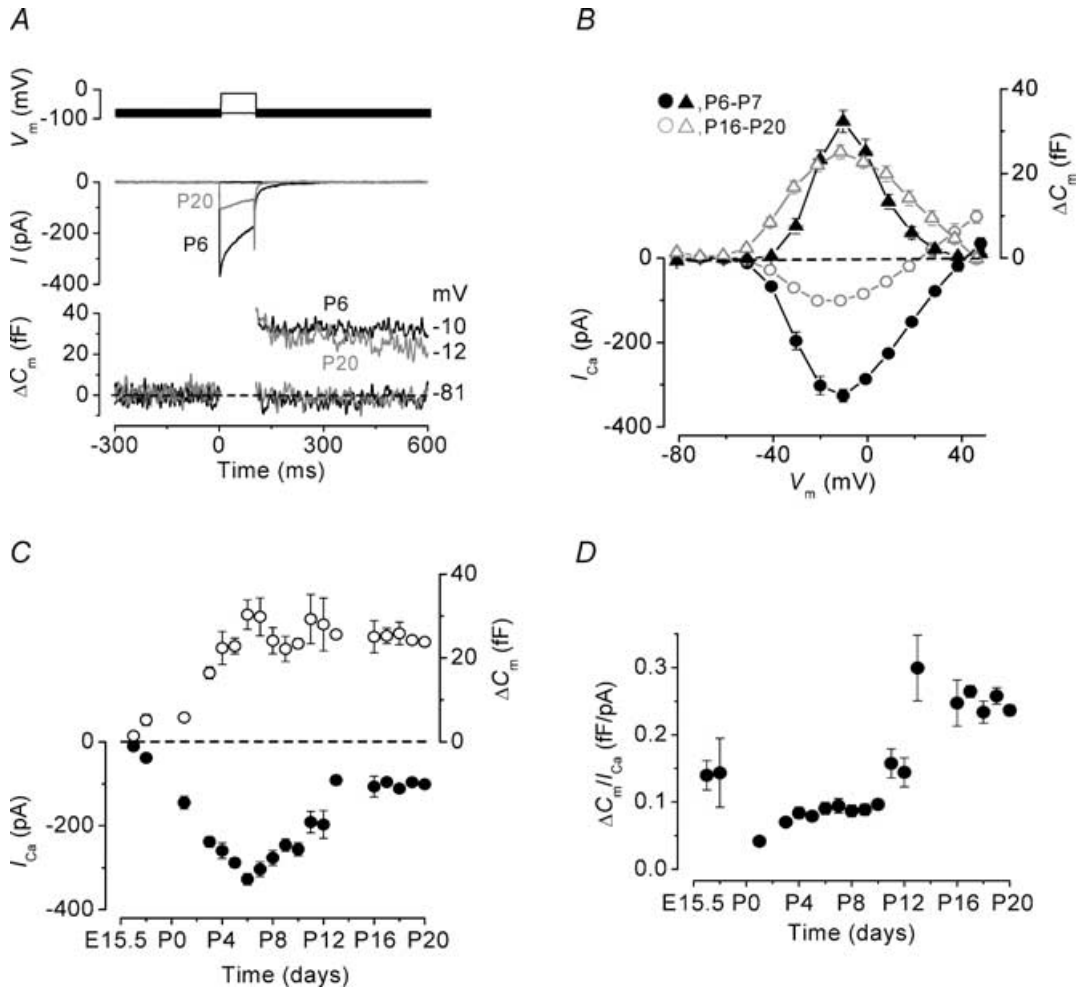

Figure 2. Comparison of I_{Ca} and ΔC_m responses during IHC development
A, inward current (middle panel) and ΔC_m (lower panel) responses from a P6 (black traces) and a P20 (grey traces) IHC. Recordings (unaveraged single traces) were obtained in response to 100 ms voltage steps, in 10 mV increments, from the holding potential of −81 mV. For clarity, only responses to two voltage steps (top panel) are shown and the membrane potentials reached are indicated to the right of the ΔC_m traces. P6, C_m 7.0 pF; R_s 6.9 MΩ; g_{leak} 1.3 nS. P20, C_m 8.7 pF; R_s 5.3 MΩ; g_{leak} 3.1 nS. *B*, average *I–V* (lower panel, circles) and ΔC_m–V (upper panel, triangles) curves for peak I_{Ca} and ΔC_m measured at each voltage step potential in immature (P6–P7, $n = 8$; black closed symbols) and mature (P16-P20, $n = 8$; grey open symbols) IHCs. *C*, average ΔC_m (upper panel) and peak I_{Ca} (lower panel) responses from IHCs at each stage of development following a 100 ms voltage step to around −11 mV. *D*, changes in the Ca^{2+} efficiency of exocytosis during development where all ΔC_m values have been normalized to I_{Ca}, in response to a voltage step to around −11 mV. Numbers of cells in *C* and *D* are (E16.5–P20): 3, 2, 3, 7, 11, 15, 21, 14, 7, 10, 15, 9, 5, 4, 3, 4, 5, 8, 3.

significantly larger ($P < 0.0001$) than that of mature cells (-98 ± 5 pA, $n = 21$). The reversal potential of the isolated I_{Ca} in mature IHCs (Fig. 3*C*) was 19 mV more positive than that obtained when I_{Ca} was recorded simultaneously with ΔC_m (Fig. 2*B*), most likely due to a more complete block of the outward K^+ currents, which would be especially important for large depolarizing voltage steps. Such a discrepancy was not apparent for the immature IHCs. This more effective block of the K^+ currents of mature IHCs was achieved by superfusing a solution containing IbTx, linopirdine and 4-AP, in addition to TEA (see Methods). The activation curves of Fig. 3*D* were obtained from the normalized chord conductance (Zidanic & Fuchs, 1995; Marcotti *et al.* 2003*b*), using reversal potentials from the fits in Fig. 3*C*, and approximated by a first-order Boltzmann equation:

$$g = \frac{g_{max}}{1 + \exp\left(\frac{V_{1/2} - V}{S}\right)} \quad (3)$$

where g is the chord conductance and the other parameters are as in eqn (2). In immature IHCs I_{Ca} activated positive to -63 mV (defined as 1% of g_{max}), 4 mV more hyperpolarized than that of mature cells (-59 mV). An example of the rapid activation of I_{Ca} in immature and mature cells is shown in detail in Fig. 3*E*. The time constants of

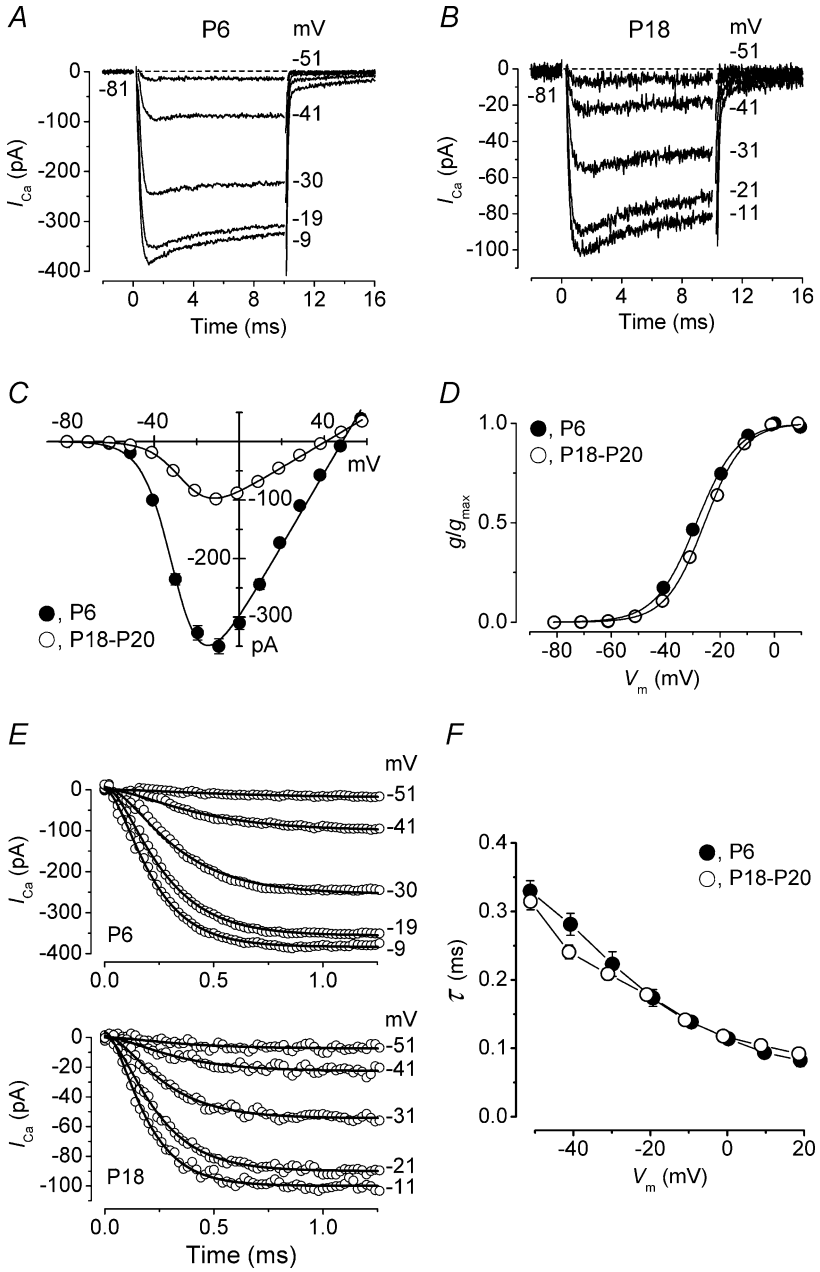

Figure 3. Properties of I_{Ca} in immature and mature IHCs

A and *B*, I_{Ca} recorded from a P6 and a P18 IHC in response to 10 ms voltage steps from -81 mV in nominal 10 mV increments; for clarity only five traces are shown. Actual test potentials reached are shown next to the traces. Recordings are averaged from seven (●, P6) and eight (○, P18) protocol repetitions. Residual capacitative transients have been blanked. P6, C_m 8.6 pF; R_s 4.0 MΩ; g_{leak} 0.9 nS. P18, C_m 10.9 pF; R_s 5.1 MΩ; g_{leak} 1.3 nS. *C*, average peak *I–V* curves for I_{Ca} at the different test potentials from immature (P6, $n = 14$) and mature (P18–P20, $n = 21$) IHCs. Continuous lines are fits obtained using eqn (2) for immature (g_{max} 7.1 nS, V_{rev} +48 mV, $V_{1/2}$ −29.3 mV, S 7.2 mV) and mature (g_{max} 3.8 nS, V_{rev} +41 mV, $V_{1/2}$ −25.2 mV, S 7.5 mV) cells. *D*, activation of I_{Ca} obtained by plotting the normalized chord conductance against the test potential. Same cells as for panel *C*. Continuous lines are fits obtained using eqn (3) for immature (g_{max} 7.1 nS, $V_{1/2}$ −28.7 mV, S 7.5 mV) and mature (g_{max} 3.8 nS, $V_{1/2}$ −25.6 mV, S 7.1 mV) cells. $V_{1/2}$ was slightly but significantly ($P < 0.0001$) different between immature and mature IHCs. *E*, upper and lower panels show the I_{Ca} traces of *A* and *B* on an expanded time scale. Continuous lines are fits to the current traces obtained using eqn (4).

F, average time constants of activation obtained from the fits to the current traces at different membrane potentials for immature (●, $n = 9$) and mature (○, $n = 14$) IHCs.

I_{Ca} activation were obtained by fitting the traces with the following equation:

$$I_{Ca}(t) = I_{max}(1 - \exp(-t/\tau)^{\alpha}) \quad (4)$$

where $I_{Ca}(t)$ is I_{Ca} at time t, I_{max} the peak I_{Ca}, τ the time constant of activation and α is 2, which gives a better fit than a power of 3, consistent with a Hodgkin–Huxley model with two opening gating particles (Hodgkin & Huxley, 1952). The time constants of I_{Ca} were not significantly different between immature and mature IHCs (Fig. 3*F*). We conclude from these experiments that the kinetic properties of I_{Ca} do not appreciably change during IHC development.

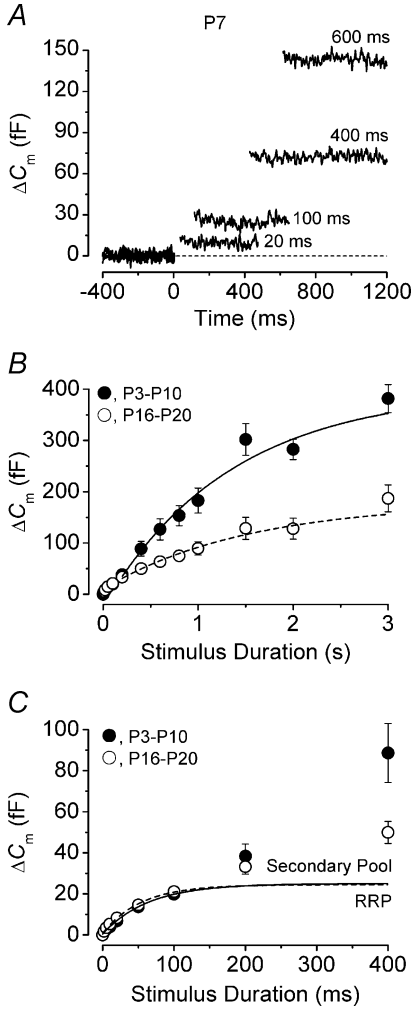

Figure 4. Developmental changes in the kinetics of neurotransmitter release
A, ΔC_m recordings (single traces) from a P7 IHC in response to voltage steps of different duration, shown next to the traces, to around −11 mV. C_m 8.4 pF; R_s 5.7 MΩ; g_{leak} 0.7 nS. *B*, average ΔC_m values obtained for each voltage step duration (2 ms to 3 s) from immature (●, P3–P10, $n = 28$) and mature (○, P16–P20, $n = 8$) IHCs. P3–P10 and P16–P20 were chosen since the $\Delta C_m/I_{Ca}$ ratios shown in Fig. 2*D* were very similar within each range. The lines are exponential fits to immature (solid line) and mature (broken line) ΔC_m values from 200 ms to 3 s. *C*, average ΔC_m values from *B* for stimulus durations up to 400 ms on an expanded time scale. ΔC_m responses from immature and mature cells showed an initial foot region over the first 100 ms that could be approximated with an exponential function (immature: solid line; mature: broken line). The RRP (below the exponential fits) and secondary pool (above the exponential fits) are indicated.

Developmental changes in the dynamics of vesicle pool recruitment in IHCs

Differences in the size, kinetics and Ca^{2+} dependence of distinct vesicle pools have previously been studied in mouse IHCs during development (Moser & Beutner, 2000; Beutner & Moser, 2001) using unphysiological recording conditions (10 mM Ca^{2+} and at room temperature). Therefore, as the results may not be representative of exocytosis in the physiological condition we have reinvestigated these properties using 1.3 mM extracellular Ca^{2+} and at body temperature.

Changes in the kinetics of neurotransmitter release were investigated using voltage steps, from 2 ms to 3 s in duration, to around −11 mV from the holding potential of −81 mV. By using stimuli of increasing duration, the emptying of different synaptic vesicle pools could be followed. Previous studies (Moser & Beutner, 2000; Beutner & Moser, 2001) have shown, using a similar voltage protocol, that in response to short (∼10 ms) stimuli there is an initial small component of ΔC_m increase, which is likely to represent the exocytosis of the RRP of vesicles docked at the active zones. The same studies have also shown that ΔC_m continues to increase at a slower rate for stimulus durations of up to 1 s. This slower component of exocytosis is likely to represent the release of vesicles from a secondary pool that is located further from the Ca^{2+} channels (von Gersdorff *et al.* 1996; von Gersdorff & Matthews, 1999; Voets *et al.* 1999).

Figure 4*A* shows ΔC_m from a P7 IHC in response to depolarizing voltage steps of varying duration. The capacitance responses to voltage steps of different duration from immature (P3–P10, $n = 28$) and mature (P16–P20, $n = 8$) IHCs are shown in Fig. 4*B*. Figure 4*C* shows that when 1.3 mM Ca^{2+} is used instead of 10 mM Ca^{2+}, voltage steps of up to about 100 ms are likely to recruit mainly the RRP in both immature and mature IHCs, since the ΔC_m increase (up to 100 ms) could be well fitted using a single exponential (P3–P10: $\tau = 64.3$ ms, maximal $\Delta C_m = 25.0$ fF; P16–P20: $\tau = 53.4$ ms, maximal $\Delta C_m = 24.5$ fF). The exponential fits of Fig. 4*C* give an indication of an RRP in immature and mature IHCs consisting of 680 and 660 synaptic vesicles and initial release rates of 389 fF s^{-1} (10 500 vesicles s^{-1}) and 459 fF s^{-1} (12 400 vesicles s^{-1}), respectively. A slower additional component of ΔC_m increase, most likely

associated with the secondary releasable pool, became evident for voltage steps from around 200 ms. A previous study showed that a relatively high concentration of 5 mM intracellular EGTA was required to isolate the RRP from the slower secondary vesicle pool when 10 mM extracellular Ca^{2+} was used (Moser & Beutner, 2000). Here we show that in 1.3 mM Ca^{2+} the RRP could be isolated using 1 mM intracellular EGTA for stimulus durations of up to 100 ms. The ΔC_m responses over the entire range of stimulus durations (2 ms to 3 s) could not be accurately approximated with a double exponential, possibly due to the delayed induction of the secondary vesicle pool (Figs 4*B* and *C*). The single exponential fits (Fig. 4*B*) to the slower component of ΔC_m from 200 ms to 3 s (P3–P10 $\tau = 1.3$ s, maximal $\Delta C_m = 360$ fF; P16–P20 $\tau = 1.5$ s, maximal $\Delta C_m = 147$ fF) gave an indication of maximal release rates of the secondary pool of around 267 fF s^{-1} (7200 vesicles s^{-1}) in immature cells and a slower rate of 96 fF s^{-1} (2600 vesicles s^{-1}) in mature cells.

The calcium dependence of distinct vesicle pools

The relation between Ca^{2+} entry and exocytosis (Fig. 5*A*) for immature (E17.5–P3 and P6–P7) and mature (P16–P20) IHCs, estimated using a synaptic transfer function (Augustine *et al.* 1985), was obtained by plotting ΔC_m against the peak I_{Ca} for 100 ms voltage steps (in order to elicit mainly the RRP of vesicles) from the holding potential to a range of potentials between –61 mV and −11 mV. The peak I_{Ca} was preferred rather than its time integral (Beutner & Moser, 2001) because the recordings were contaminated by the residual unblocked slower activating SK Ca^{2+}-activated K^+ current in immature IHCs (Marcotti *et al.* 2003*b*), and $I_{K,s}$ in mature IHCs (Marcotti *et al.* 2003*a*, 2004), which are likely to be responsible for the apparent large inactivation of the inward current. Since the slower activation of these currents does not affect the peak of the much faster I_{Ca} we decided that this was the most accurate representation of Ca^{2+} entry into immature and mature IHCs. Data were approximated using a power function:

$$\Delta C_m \propto I_{Ca}^N \quad (5)$$

where N is the power. The three transfer functions obtained using eqn (5) equate to straight lines when plotted on double-logarithmic coordinates (Fig. 5*B*). The average power obtained from the transfer functions of immature IHCs (E17.5–P3: 3.30 ± 0.11, $n = 12$; P6–P7: 3.34 ± 0.11, $n = 8$) indicates that each release event requires a minimum of four Ca^{2+} binding steps to occur (Dodge & Rahamimoff, 1967; Cohen & Van der Kloot, 1985). Somewhat surprisingly, the transfer function obtained from mature IHCs was best approximated using a power of 0.70 ± 0.02 ($n = 8$, P16-P20), significantly ($P < 0.0001$) smaller than that of immature cells, suggesting a near linear relation between Ca^{2+} entry and exocytosis (Llinas *et al.* 1976, 1981). The broken line in Fig. 5*A* and *B* represents the maximum size of the predicted RRP (from the exponential fits in Fig. 4*C*), and this indicates that 100 ms voltage steps in 1.3 mM Ca^{2+} elicit the release of vesicles mainly within the RRP. Therefore, the Ca^{2+} dependence indicated by the synaptic transfer functions (Fig. 5*A* and *B*) reflects mainly that of the RRP at all stages shown.

The developmental change in Ca^{2+} dependence of the RRP and secondary vesicle pools was investigated further by stimulating immature and mature IHCs with a 100 ms voltage step to a potential that elicited maximal responses (near −11 mV) from −81 mV while varying the extracellular Ca^{2+} concentration (Fig. 6). With the use of high extracellular Ca^{2+} concentrations, the resulting

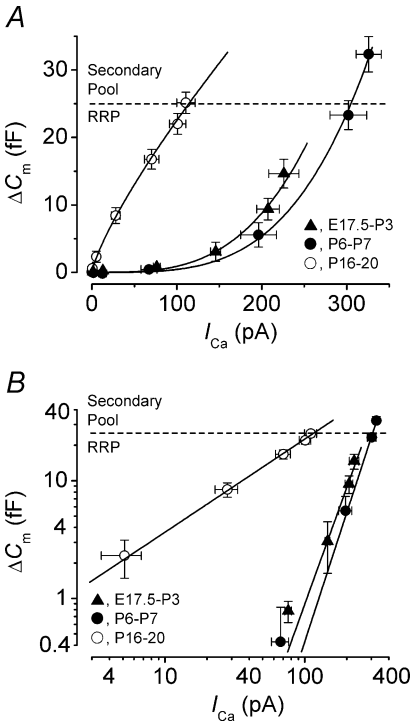

Figure 5. Synaptic transfer functions relating I_{Ca} and ΔC_m at different membrane potentials
A, average ΔC_m responses from E17.5–P3 (▲, $n = 12$), P6–P7 (●, $n = 8$) and P16–P20 (○, $n = 8$) IHCs plotted against the corresponding absolute I_{Ca} magnitude resulting from 100 ms voltage steps from the holding potential of −81 mV to different voltages up to around −11 mV in nominal 10 mV increments. For immature (P6–P7) and mature (P16–P20) IHCs, the data are from the I–V and ΔC_m–V curves shown in Fig. 2*B*. Solid lines are fits to data points according to eqn (5) with powers N of: E17.5–P3, 3.3; P6–P7, 3.3; P16–P20, 0.7. The broken horizontal lines (also in *B*) represent the maximum size of the predicted RRP (from Fig. 4*C*). *B*, I_{Ca} and ΔC_m responses as *A* but plotted using double-logarithmic coordinates. Straight lines are the same functions used in *A* with the same parameters.

larger I_{Ca} allowed us to determine the Ca^{2+} dependence of the secondary vesicle pool to a greater extent. These experiments also allow a direct comparison between this and previous studies on hair cells where ΔC_m responses have been recorded using different extracellular Ca^{2+} concentrations (4 mM Ca^{2+}: Parsons *et al.* 1994; 5 mM Ca^{2+}: Spassova *et al.* 2001; 10 mM Ca^{2+}: Moser & Beutner, 2000; Beutner & Moser, 2001). Figure 6*A* shows the ΔC_m responses near −11 mV, from four immature IHCs in different external Ca^{2+} concentrations. When 10 mM extracellular Ca^{2+} was used, the IHCs rapidly deteriorated, therefore no more than one viable cell was recorded for each dissected organ of Corti. Changing the Ca^{2+} concentration over the range from zero to 10 mM significantly ($P < 0.0001$ in all cases) increased both I_{Ca} (Fig. 6*B*) and ΔC_m (Fig. 6*C*) in immature and mature IHCs. The individual data points were fitted using the following equation, which assumes the independent

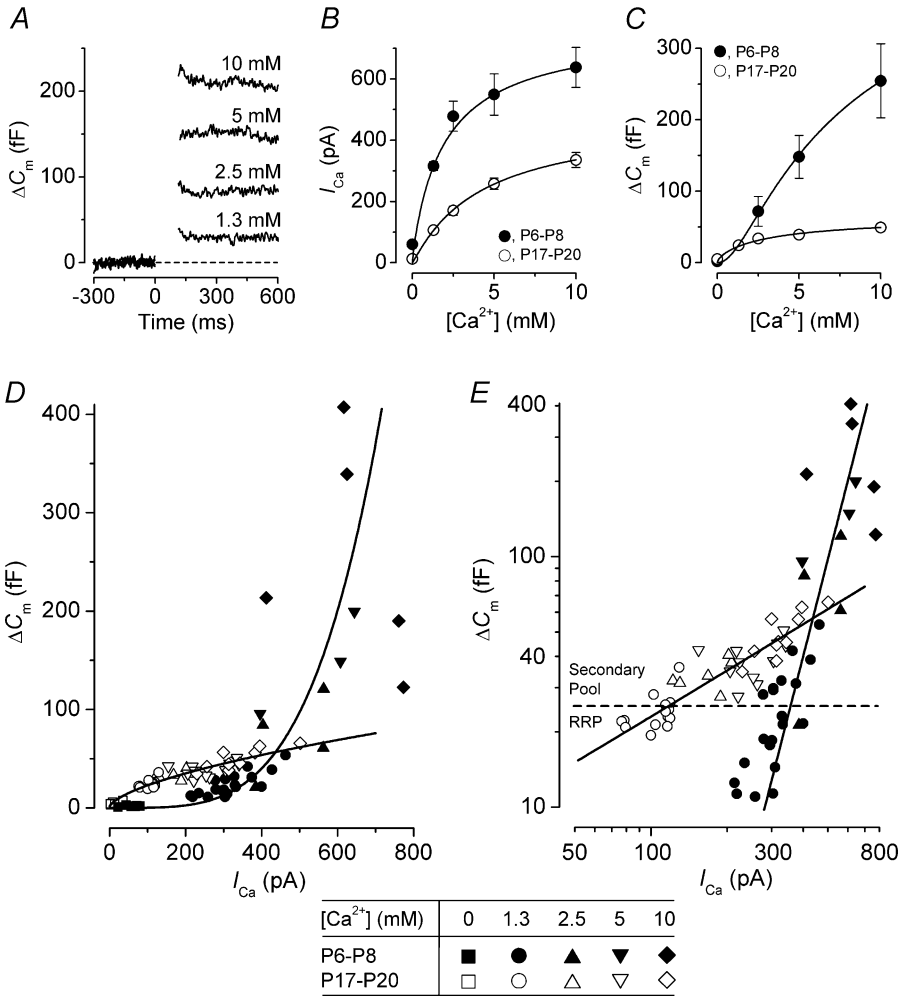

Figure 6. Dependence of I_{Ca} and ΔC_m on extracellular Ca^{2+}
A, ΔC_m (single traces) from four immature IHCs in different extracellular Ca^{2+} concentrations (indicated above each trace) in response to a 100 ms voltage step to around −11 mV. 1.3 mM (P8), C_m 9.9 pF; R_s 4.3 MΩ; g_{leak} 1.4 nS. 2.5 mM (P6), C_m 8.0 pF; R_s 5.0 MΩ; g_{leak} 0.7 nS. 5 mM (P7), C_m 8.1 pF; R_s 6.6 MΩ; g_{leak} 1.1 nS. 10 mM (P6), C_m 8.0 pF; R_s 5.6 MΩ; g_{leak} 1.4 nS. *B* and *C*, peak I_{Ca} magnitudes and corresponding ΔC_m, respectively, as a function of extracellular Ca^{2+} for immature (●, P6–P8) and mature (○, P17–P20) IHCs. Numbers of cells at each concentration are: immature, 8 (0 mM), 20 (1.3 mM), 4 (2.5 mM), 3 (5 mM) and 5 (10 mM); mature, 5 (0 mM), 18 (1.3 mM), 6 (2.5 mM), 11 (5 mM) and 10 (10 mM). Solid lines are fits according to eqn (6) (see Results). *D*, synaptic transfer functions relating I_{Ca} and ΔC_m where ΔC_m values for each cell at different Ca^{2+} concentrations are plotted against their corresponding I_{Ca} magnitude for immature (filled symbols) and mature (open symbols) IHCs. Immature and mature data points are fit (solid lines) using eqn (5) with powers *N* of: 3.97 (immature) and 0.62 (mature). *E*, as *D* but plotted using double-logarithmic coordinates. Straight lines are the same functions used in *D* with the same parameters. The Ca^{2+}-free data points shown in *D* have been omitted. The broken horizontal line represents the maximum size of the predicted RRP (from Fig. 4*C*).

action of n Ca^{2+} binding sites (Augustine & Charlton, 1986):

$$y \propto \left(\frac{[Ca]_O}{1 + \frac{[Ca]_O}{K_D}} \right)^n \quad (6)$$

where y is I_{Ca} (Fig. 6*B*) or ΔC_m (Fig. 6*C*), $[Ca]_O$ the extracellular Ca^{2+} concentration, K_D the dissociation constant for Ca^{2+} and n the order of the Ca^{2+}-dependent reaction. The values for n and K_D obtained from the fits were: immature I_{Ca}, 0.85 and 2.4 mM; immature ΔC_m, 2.47 and 3.1 mM; mature I_{Ca}, 1.11 and 3.8 mM; mature ΔC_m, 0.64 and 5.3 mM. The estimates for K_D were independently verified using linear fits in double reciprocal (Lineweaver–Burk) plots (not shown) of the n^{th} root of I_{Ca} or ΔC_m against the extracellular Ca^{2+} concentration (Dodge & Rahamimoff, 1967). Using this plotting method the values for K_D obtained from the x-axis intercepts were in all cases within 0.3 mM of those quoted above. The similar order of the Ca^{2+} dependence of I_{Ca} ($n \approx 1$) in both immature and mature IHCs (Fig. 6*B*) suggests that Ca^{2+} entry through the Ca^{2+} channels does not significantly contribute to the different power relations of exocytosis observed in these cells (Fig. 5). Instead, this developmental reduction in the power relation between I_{Ca} and exocytosis is likely to be caused by a reduced Ca^{2+} dependence of a step beyond Ca^{2+} entry as indicated by the different n-values for ΔC_m in Fig. 6*C*. The direct relation between I_{Ca} and exocytosis (Fig. 6*D* and *E*) can be obtained by plotting synaptic transfer functions like those of Fig. 5, but now using maximum responses obtained near −11 mV in different Ca^{2+} concentrations from individual cells that have been used for the averages shown in Figs 6*B* and *C*. The immature and mature synaptic transfer functions were approximated using powers of 3.97 and 0.62, respectively, close to those obtained in Fig. 5. This result indicates that the relation between ΔC_m and I_{Ca} at both immature and mature stages is not affected by the different methods (changing either membrane potential or extracellular Ca^{2+}) used to vary Ca^{2+} entry. Studies investigating the Ca^{2+} dependence of exocytosis at the squid giant synapse have shown that a power of around 4 was obtained when I_{Ca} was varied either by using voltage steps to different membrane potentials (Augustine *et al.* 1985) or by changing extracellular Ca^{2+} over a range of concentrations between 1 mM and 50 mM (Augustine & Charlton 1986). For extracellular Ca^{2+} concentrations lower than the K_D (i.e. if $[Ca]_O/K_D < 1$ in eqn (6)) eqn (6) approximates to a power function for both I_{Ca} and ΔC_m:

$$y \propto [Ca]_O^n \quad (7)$$

By combining eqn (7) for both I_{Ca} and ΔC_m the $[Ca]_O$ term is eliminated and the following power function obtained:

$$\Delta C_m \propto (I_{Ca})^{n_{\Delta Cm}/n_{ICa}} \quad (8)$$

where $n_{\Delta Cm}$ and n_{ICa} are the n-values for ΔC_m and I_{Ca}, respectively, from eqn (7). Note that eqn (8) is formally equivalent to eqn (5). This approach could be applied reasonably well to IHCs since the average K_D from Figs 6*B* and *C* was around 4 mM, a value larger than the physiological extracellular Ca^{2+} concentration (1.3 mM). In immature and mature IHCs the values for $n_{\Delta Cm}/n_{ICa}$ (Figs 6*B* and *C*) were 2.91 and 0.58, respectively, which are similar to the powers N (eqn 5) of 3.97 and 0.62 obtained in Figs 6*D* and *E*. The method of simplifying eqn (6) is only used here to give an indication of the relationship between extracellular Ca^{2+} and transmitter release. We found that the most consistent way of measuring the Ca^{2+} dependency of exocytosis was to plot the actual I_{Ca} against ΔC_m (Figs 5 and 6*D* or *E*), which is indicated by the similarity of the N-values obtained even though different methods were used to vary I_{Ca}. Even so, the dependence of I_{Ca} and ΔC_m on extracellular Ca^{2+} seems to be sufficient to account for the different synaptic transfer curves of immature and mature IHCs, especially around the physiological range of Ca^{2+} concentrations.

The maximum size of the predicted RRP (indicated in Fig. 6*E*) suggests that 100 ms stimulation to around −11 mV, in extracellular Ca^{2+} concentrations >1.3 mM, generally elicits the release of the entire RRP and, to a varying extent, the secondary vesicle pool. Therefore, the synaptic transfer functions (Fig. 6*E*) reflect the Ca^{2+} dependence of both the RRP and secondary pools in immature and mature IHCs, and imply that there is a developmental modification of the release mechanism that controls the exocytosis of vesicles from both the RRP and secondary pools. The lower Ca^{2+} dependence of both vesicle pools in mature IHCs (Figs 5*B* and 6*E*) could perform a dual role by allowing more efficient release of the RRP at the lower range of I_{Ca} (Fig. 5*B*), while providing a more gradual recruitment of the secondary pool at higher I_{Ca} (Fig. 6*E*) or during prolonged stimulation (>100 ms, Fig. 4*B*).

Discussion

Much information regarding neurotransmitter release from mouse IHCs onto afferent terminals has been provided in recent years (Moser & Beutner, 2000; Beutner & Moser, 2001; Beutner *et al.* 2001), although the recording conditions used in these studies were largely unphysiological (room temperature and 10 mM extracellular Ca^{2+}). Since exocytosis is a Ca^{2+}-dependent process we investigated this phenomenon in 1.3 mM Ca^{2+} and at body temperature to provide further insights into exocytosis in mammalian IHCs.

The Ca^{2+} efficiency of IHC exocytosis

The amplitudes of I_{Ca} and ΔC_m increased during development up until P6, when either voltage steps or spike

protocols were used. At E16.5 a single spike elicited a small I_{Ca} and a ΔC_m response that corresponded to the fusion of around 15 vesicles (Fig. 1). At P6 the number of vesicles per spike increased to about 310. The similar developmental trend between I_{Ca} and ΔC_m (Fig. 1*E*) suggests that the synaptic machinery is fully functional from embryonic stages and the degree of release is governed by the development of I_{Ca}. Although the amplitude of I_{Ca} changed during development (Fig. 2*C*), its activation kinetics did not appreciably differ between immature and mature IHCs (Fig. 3). These results, together with the observation that the α1D ($Ca_v1.3$) Ca^{2+} channel subunit is responsible for >90% of I_{Ca} at both stages of development (Platzer *et al.* 2000; Brandt *et al.* 2003), indicate that the decline in I_{Ca} from P6 is due to a reduction in the number of Ca^{2+} channels rather than a change in channel composition.

After P6, while I_{Ca} declined to reach a steady value from about P13, ΔC_m did not change significantly (Fig. 2*C*). The relatively stable ΔC_m responses from P6, together with the decline in I_{Ca} obtained in 1.3 mM extracellular Ca^{2+}, increased the Ca^{2+} efficiency of exocytosis, reaching statistical significance from P11 (Fig. 2*D*). Theoretically, if only Ca^{2+} channels that are not coupled to exocytosis would become eliminated with IHC maturation, this would give a false impression of an increase in Ca^{2+} efficiency. However, this is unlikely since extrasynaptic Ca^{2+} channels remain in mature IHCs (Hafidi & Dulon, 2004). A higher Ca^{2+} efficiency in mature IHCs compared to that of immature cells has previously been shown, using 10 mM Ca^{2+}, only when I_{Ca} was elicited using short voltage steps (up to about 10 ms, Beutner & Moser, 2001) most likely due to the earlier recruitment of the secondary pool of vesicles (see below) in high extracellular Ca^{2+}. Indeed, when unphysiologically high Ca^{2+} concentrations (>1.3 mM) were used, the smaller I_{Ca} in mature cells (Fig. 6*B*) was now accompanied by a simultaneous reduction in ΔC_m (Fig. 6*C*) consistent with previous observations (Beutner & Moser, 2001). The increased Ca^{2+} efficiency of exocytosis with IHC maturation (Fig. 2*D*) could be due to an altered spatial relationship between Ca^{2+} entry and the release machinery, a manifestation of which may be the change in ribbon synapse morphology from spherical to plate-like (Sobkowicz *et al.* 1982; Liberman, 1980). Alternatively or additionally, the expression of molecules such as the Ca^{2+}-binding protein synaptotagmin (Geppert *et al.* 1994) or the cysteine-string protein (Eybalin *et al.* 2002), thought to improve stimulus–secretion coupling (Chamberlain & Burgoyne, 2000), could be responsible for the increased Ca^{2+} efficiency. An enhancement of exocytotic Ca^{2+} efficiency has also been correlated with developmental changes in calyx of Held ultrastructure (Taschenberger *et al.* 2002). Whatever the developmental alteration turns out to be, it is also likely to be responsible for the changes in Ca^{2+} dependence as discussed in the next section.

The Ca^{2+} dependence of vesicle pool exocytosis

Vesicle exocytosis in excitable cells typically has a high-order dependence on presynaptic Ca^{2+} entry (Dodge & Rahamimoff, 1967; Augustine & Charlton, 1986). However, in the mouse cochlea this applies only to immature IHCs in which the relation between I_{Ca} and ΔC_m was approximated by a power of about four, compared to 0.7 in mature cells (Figs 5 and 6), indicating that each release event requires the binding of around four and one Ca^{2+} ions, respectively. The change in Ca^{2+} dependence of exocytosis during development was evident for both the RRP and secondary pools (Fig. 6*E*), implying that a common release mechanism exists for both pools. An approximately linear relation between presynaptic I_{Ca} and transmitter release has been reported in previous studies (Llinas *et al.* 1976, 1981) although it has been suggested that the high extracellular Ca^{2+} concentrations of between 3 mM and 100 mM that were used in these studies could be responsible for the linearity (Augustine & Charlton, 1986). However, this possibility seems unlikely to apply to mature IHCs since a nearly linear Ca^{2+} dependence of exocytosis was also observed in physiological 1.3 mM Ca^{2+} (Fig. 5*A*). An alternative explanation for the reduced Ca^{2+} dependence in mature cells could be an increased resting intracellular Ca^{2+} caused by local buffer saturation (Cohen & Van der Kloot, 1985). Such a situation might potentially arise from damage to mature IHCs, which are considered to be more fragile than at immature stages, during tissue preparation, which would increase their leak conductance and cause them to become permanently depolarized. This might, in turn, activate a proportion of voltage-gated Ca^{2+} channels and result in an increased resting intracellular Ca^{2+} concentration. However, using the same preparation (Marcotti *et al.* 2003*a*), we found that the resting membrane potential of IHCs older than P8 (-74.4 ± 0.7 mV, $n = 34$, P8–P30) was significantly ($P < 0.0001$) more negative than that at earlier stages (-54.9 ± 0.6 mV, $n = 70$, P0–P7), suggesting that the cells are in good condition and that the resting intracellular Ca^{2+} level is not higher than at immature stages. One possibility that remains is that the local concentration of fixed buffers might be reduced during maturation.

A previous study on mature mouse IHCs (Beutner *et al.* 2001) estimated, using flash photolysis of caged Ca^{2+}, five co-operative Ca^{2+} binding steps for each release event. However, flash photolysis recruits a pool of vesicles that is two orders of magnitude larger (Beutner *et al.* 2001) than the RRP activated by Ca^{2+} influx through Ca^{2+} channels and likely to be on average further removed from the active zones. This larger pool may not be coupled to synaptic proteins (Wiser *et al.* 1999), may experience a

lower resting Ca^{2+} concentration than the RRP, and is probably not involved in IHC exocytosis over the physiological range of intracellular Ca^{2+} (Beutner *et al.* 2001). A linear relation between I_{Ca} and exocytosis in physiological extracellular Ca^{2+} has also recently been demonstrated at the photoreceptor synapse (Thoreson *et al.* 2004). The same study has also shown a near-linear relation between the rate of exocytosis and intracellular Ca^{2+} using flash photolysis when Ca^{2+} elevations were kept within the expected physiological range at the active zones (0.7 μM to 3 μM). However, a third-order Ca^{2+} dependency better described the data obtained over the entire range of intracellular Ca^{2+} concentrations investigated (0.2 μM to 5 μM, Thoreson *et al.* 2004). Similar considerations might explain the discrepancy between the linear Ca^{2+} dependence of mature IHCs in the present study and the fifth-order relation described by Beutner *et al.* (2001) that was measured over a range of very high intracellular Ca^{2+} concentrations (7 μM to 110 μM).

The power relation between ΔC_m and I_{Ca} could reflect a number of steps along the excitation–exocytosis cascade and therefore one or more of these steps could contribute to the linearization in the Ca^{2+} dependence of exocytosis with IHC development. Changes in the proportion of Ca^{2+} channels contributing to neurotransmitter release or the coupling between Ca^{2+} channels and release sites could be responsible for this linearization. The former is unlikely because even if only a proportion of the total number of Ca^{2+} channels in immature cells were able to influence release (Rodriguez-Contreras & Yamoah, 2001), the similar voltage dependence of I_{Ca} in both immature and mature cells (Fig. 3*C*), that is mainly (>90%) determined by L-type Ca^{2+} channels at both stages (Platzer *et al.* 2000; Brandt *et al.* 2003), would generate the same overall Ca^{2+} dependence of exocytosis, even if I_{Ca} was reduced by any fraction. In mature IHCs, a very efficient coupling between Ca^{2+} channels and release sites could ensure that high Ca^{2+} concentrations are reached around the active zones, thus forcing the exocytotic mechanisms to operate at a range where the Ca^{2+} dependence becomes more linear (Dodge & Rahamimoff, 1967; Cohen & Van der Kloot, 1985). This more efficient coupling could arise from a closer colocalization between Ca^{2+} channels and release sites, or a change in the Ca^{2+} sensing molecules of exocytosis during IHC maturation. The Ca^{2+} sensor of exocytosis is generally believed to be synaptotagmin (Geppert *et al.* 1994; Koh & Bellen, 2003). This protein is integrated into the membrane of synaptic vesicles, is found in multiple isoforms with different Ca^{2+}-binding properties (Südhof & Rizo, 1996; Südhof, 2002), and has been shown to form heteromultimers (Chapman *et al.* 1998). A reduced Ca^{2+} dependence of exocytosis was observed in the presence of synaptotagmin IV (Littleton *et al.* 1999) or mutations in a Ca^{2+}-binding domain of synaptotagmin I (Littleton *et al.* 1994), both of which reduced the total number of Ca^{2+}-binding sites. Although the expression of synaptotagmin IV has been demonstrated in mature guinea-pig hair cells (Safieddine & Wenthold, 1999), its presence is yet to be determined in the immature cochlea.

The kinetic properties of IHC exocytosis

Two kinetically distinct synaptic vesicle pools have been observed in sensory cells such as hair cells and photoreceptors (von Gersdorff & Matthews, 1999; Lenzi & von Gersdorff, 2001): an RRP of vesicles that are docked at the active zones and represent a small and rapid initial component of exocytosis, and a much slower but larger secondary pool representing the release of vesicles that are probably attached to the synaptic ribbon but located further away from the active zone. The synaptic ribbon architecture of sensory receptors appears to be a determinant of vesicle pool size and release kinetics (Lenzi & von Gersdorff, 2001; von Gersdorff, 2001; Parsons & Sterling, 2003; Fuchs *et al.* 2003).

The size and kinetics of the RRP remained relatively constant during postnatal development (Fig. 4*C*), consistent with a previous study (Beutner & Moser, 2001). While the kinetics of RRP release were slower than those obtained in high Ca^{2+} (Beutner & Moser, 2001), the estimated size of the RRP (670 vesicles) in immature and mature cells in the present study was 2.3 times larger than that reported by Beutner & Moser (2001). The possibility that the larger estimated RRP had been partially affected by the much slower secondary pool appears unlikely because this slower component was only recruited for steps longer than 100 ms in both immature and mature cells. Moreover, the rapidly releasable component (up to 100 ms, Fig. 4*C*) has been shown to be resistant to high concentrations of the slow Ca^{2+} buffer EGTA that affect the much slower secondary pool (Moser & Beutner, 2000). Finally, if the secondary pool was contaminating the RRP measurement (i.e. >100 ms in Fig. 4*B*), the amplitude of ΔC_m would decline with IHC development due to the three-fold slower secondary pool release rate in mature cells. Therefore, the constant ΔC_m responses in Fig. 2*C*, from P6 onwards, provide further support for the release of only the RRP following 100 ms voltage steps in physiological extracellular Ca^{2+}.

Physiological implications of developmental changes in Ca^{2+} efficiency and Ca^{2+} dependence of exocytosis

Immature IHCs (E18.5–P6) generate spontaneous action potentials whereas mature cells respond to sound with graded receptor potentials. The properties of synaptic transmission change during maturation such that immature IHCs only release neurotransmitter in response to an action potential, while mature IHCs are capable of continuous vesicle release *in vivo*, both spontaneously

and in response to small changes in membrane potential (Sewell, 1996). The high Ca^{2+} efficiency of transmitter release by mature IHCs would promote spontaneous neurotransmitter release whereas the low, near-linear, Ca^{2+} dependence would lead to a broadening of their dynamic range by allowing the cells to respond efficiently to both small and large stimuli, thus providing finely graded intensity discrimination over a wide dynamic range of sound stimuli. Interestingly, a linear relation between Ca^{2+} entry and exocytosis is also responsible for the high-fidelity transmission of small changes in receptor potential at sensory synapses of the photoreceptor (Thoreson *et al.* 2004) and olfactory receptor neurones (Murphy *et al.* 2004). On the other hand, the large I_{Ca}, lower Ca^{2+} efficiency and steeper Ca^{2+} dependence of exocytosis by immature IHCs may be specializations to ensure that the cells can fire action potentials and release neurotransmitter only during these spikes but not in the intervals between spikes. This would be important if spontaneous action potential activity in IHCs contributes to the maturation and refinement of synaptic connections in the developing auditory system. This possibility has been suggested on the basis of indirect evidence (Kros *et al.* 1998; Marcotti *et al.* 2003*a*). A similar fourth-power Ca^{2+} dependence to that of exocytosis by immature IHCs has generally been observed at synapses activated by action potentials (del Castillo & Katz, 1954; Dodge & Rahamimoff, 1967; Augustine *et al.* 1985; Nachshen & Sanchez-Armass, 1987; Borst & Sakmann, 1996).

References

Augustine GJ & Charlton MP (1986). Calcium dependence of presynaptic calcium current and post-synaptic response at the squid giant synapse. *J Physiol* **381**, 619–640.

Augustine GJ, Charlton MP & Smith SJ (1985). Calcium entry and transmitter release at voltage-clamped nerve terminals of squid. *J Physiol* **367**, 163–181.

Beutner D & Moser T (2001). The presynaptic function of mouse cochlear inner hair cells during development of hearing. *J Neurosci* **21**, 4593–4599.

Beutner D, Voets T, Neher E & Moser T (2001). Calcium dependence of exocytosis and endocytosis at the cochlear inner hair cell afferent synapse. *Neuron* **29**, 681–690.

Borst JG & Sakmann B (1996). Calcium influx and transmitter release in a fast CNS synapse. *Nature* **383**, 431–434.

Brandt A, Striessnig J & Moser T (2003). $Ca_V1.3$ channels are essential for development and presynaptic activity of cochlear inner hair cells. *J Neurosci* **23**, 10832–10840.

Chamberlain LH & Burgoyne RD (2000). Cysteine-string protein: the chaperone at the synapse. *J Neurochem* **74**, 1781–1789.

Chapman ER, Desai RC, Davis AF & Tornehl CK (1998). Delineation of the oligomerization, AP-2 binding, and synprint binding region of the C2B domain of synaptotagmin. *J Biol Chem* **273**, 32966–32972.

Cohen I & Van der Kloot W (1985). Calcium and transmitter release. *Int Rev Neurobiol* **27**, 299–336.

del Castillo J & Katz B (1954). The effect of magnesium on the activity of motor nerve endings. *J Physiol* **124**, 553–559.

Dodge FA & Rahamimoff R (1967). Co-operative action of calcium ions in transmitter release at the muscular junction. *J Physiol* **193**, 419–432.

Echteler SM (1992). Developmental segregation in the afferent projections to mammalian auditory hair cells. *Proc Natl Acad Sci U S A* **89**, 6324–6327.

Ehret G (1975). Masked auditory thresholds, critical ratios, and scales of the basilar membrane of the housemouse (*Mus musculus*). *J Comp Physiol* **103**, 329–341.

Engel J, Michna M, Platzer J & Striessnig J (2002). Calcium channels in mouse hair cells: function, properties and pharmacology. *Adv Otorhinolaryngol* **59**, 35–41.

Eybalin M, Renard N, Aure F & Safieddine S (2002). Cysteine-string protein in inner hair cells of the organ of Corti: synaptic expression and upregulation at the onset of hearing. *Eur J Neurosci* **15**, 1409–1420.

Fuchs PA, Glowatzki E & Moser T (2003). The afferent synapse of cochlear hair cells. *Curr Opin Neurobiol* **13**, 452–458.

Geppert M, Goda Y, Hammer RE, Li C, Rosahl TW, Stevens CF & Südhof TC (1994). Synaptotagmin I: a major Ca^{2+} sensor for transmitter release at a central synapse. *Cell* **79**, 717–727.

Glowatzki E & Fuchs PA (2002). Transmitter release at the hair cell ribbon synapse. *Nat Neurosci* **5**, 147–154.

Hafidi A & Dulon D (2004). Developmental expression of $Ca_v1.3$ (α1D) calcium channels in the mouse inner ear. *Brain Res Dev Brain Res* **150**, 167–175.

Hodgkin AL & Huxley AF (1952). A quantitative description of membrane current and its application to conduction and excitation in nerve. *J Physiol* **117**, 500–544.

Johnson SL, Thomas MV & Kros CJ (2002). Membrane capacitance measurement using patch clamp with integrated self-balancing lock-in amplifier. *Pflugers Arch* **443**, 653–663.

Koh TW & Bellen HJ (2003). Synaptotagmin I, a Ca^{2+} sensor for neurotransmitter release. *Trends Neurosci* **26**, 413–422.

Kros CJ, Ruppersberg JP & Rüsch A (1998). Expression of a potassium current in inner hair cells during development of hearing in mice. *Nature* **394**, 281–284.

Lenzi D, Runyeon JW, Crum J, Ellisman MK & Roberts WM (1999). Synaptic vesicle populations in saccular hair cells reconstructed by electron tomography. *J Neurosci* **19**, 119–132.

Lenzi D & von Gersdorff H (2001). Structure suggests function: the case for synaptic ribbons as exocytotic nanomachines. *Bioessays* **23**, 831–840.

Liberman MC (1980). Morphological differences among radial afferent fibers in the cat cochlea: an electron-microscopic study of serial sections. *Hear Res* **3**, 45–63.

Littleton JT, Serano TL, Rubin GM, Ganetzky B & Chapman ER (1999). Synaptic function modulated by changes in the ratio of synaptotagmin I and IV. *Nature* **400**, 757–760.

Littleton TJ, Stern M, Perin M & Bellen HJ (1994). Calcium dependence of neurotransmitter release and rate of spontaneous vesicle fusions are altered in *Drosophila* synaptotagmin mutants. *Proc Natl Acad Sci U S A* **91**, 10888–10892.

Llinas R, Steinberg IZ & Walton K (1976). Presynaptic calcium currents and their relation to synaptic transmission: voltage clamp study in squid giant synapse and theoretical model for the calcium gate. *Proc Natl Acad Sci U S A* **73**, 2918–2922.

Llinas R, Steinberg IZ & Walton K (1981). Relationship between presynaptic calcium current and postsynaptic potential in squid giant synapse. *Biophys J* **33**, 323–351.

Marcotti W, Johnson SL, Holley MC & Kros CJ (2003*a*). Developmental changes in the expression of potassium currents of embryonic, neonatal and mature mouse inner hair cells. *J Physiol* **548**, 383–400.

Marcotti W, Johnson SL & Kros CJ (2004). Effects of intracellular stores and extracellular Ca^{2+} on Ca^{2+}-activated K^+ currents in mature mouse inner hair cells. *J Physiol* **557**, 613–633.

Marcotti W, Johnson SL, Rüsch A & Kros CJ (2003*b*). Sodium and calcium currents shape action potentials in immature mouse inner hair cells. *J Physiol* **552**, 743–761.

Moser T & Beutner D (2000). Kinetics of exocytosis and endocytosis at the cochlear inner hair cell afferent synapse of the mouse. *Proc Natl Acad Sci U S A* **97**, 883–888.

Murphy GJ, Glickfeld LL, Balsen Z & Isaacson JS (2004). Sensory neuron signaling to the brain: properties of transmitter release from olfactory nerve terminals. *J Neurosci* **24**, 3023–3030.

Nachshen DA & Sanchez-Armass S (1987). Co-operative action of calcium ions in dopamine release from rat brain synaptosomes. *J Physiol* **387**, 415–423.

Neher E & Marty A (1982). Discrete changes of cell membrane capacitance observed under conditions of enhanced secretion in bovine adrenal chromaffin cells. *Proc Natl Acad Sci U S A* **79**, 6712–6716.

Parsons TD, Lenzi D, Almers W & Roberts WM (1994). Calcium-triggered exocytosis and endocytosis in an isolated presynaptic cell: capacitance measurements in saccular hair cells. *Neuron* **13**, 875–883.

Parsons TD & Sterling P (2003). Synaptic ribbon. Conveyor belt or safety belt? *Neuron* **37**, 379–382.

Platzer J, Engel J, Schrott-Fischer A, Stephan K, Bova S, Chen H, Zheng H & Striessnig J (2000). Congenital deafness and sinoatrial node dysfunction in mice lacking class D L-type Ca^{2+} channels. *Cell* **102**, 89–97.

Pujol R, Lavigne-Rebillard M & Lenoir M (1998). Development of sensory and neural structures in the mammalian cochlea. In *Development of the Auditory System*, ed. Rubel EW, Popper AN, Fay RR, pp. 146–192. Springer, New York.

Rodriguez-Contreras A & Yamoah EN (2001). Direct measurement of single-channel Ca^{2+} currents in bullfrog hair cells reveals two distinct channel subtypes. *J Physiol* **534**, 669–689.

Russell IJ & Sellick PM (1978). Intracellular studies of hair cells in the mammalian cochlea. *J Physiol* **284**, 261–290.

Safieddine S & Wenthold RJ (1999). SNARE complex at the ribbon synapses of cochlear hair cells: analysis of synaptic vesicle- and synaptic membrane-associated proteins. *Eur J Neurosci* **11**, 803–812.

Sewell WF (1996). Neurotransmitters and synaptic transmission. In *The Cochlea*, ed. Dallos P, Popper AN & Fay RR, pp. 503–533. Springer, New York.

Shnerson A, Devigne C & Pujol R (1982). Age-related changes in the C57BL/6J mouse cochlea. II. Ultrastructural findings. *Dev Brain Res* **2**, 77–88.

Singer D, Biel M, Lotan I, Flockerzi V, Hofmann F & Dascal N (1991). The roles of the subunits in the function of the calcium channel. *Science* **253**, 1553–1557.

Sobkowicz HM, Rose JE, Scott GE & Slapnick SM (1982). Ribbon synapses in the developing intact and cultured organ of Corti in the mouse. *J Neurosci* **2**, 942–957.

Spassova M, Eisen MD, Saunders JC & Parsons TD (2001). Chick cochlear hair cell exocytosis mediated by dihydropyridine-sensitive calcium channels. *J Physiol* **535**, 689–696.

Südhof TC (2002). Synaptotagmins: why so many? *J Biol Chem* **277**, 7629–7632.

Südhof TC & Rizo J (1996). Synaptotagmins: C2-domain proteins that regulate membrane traffic. *Neuron* **17**, 379–388.

Taschenberger H, Leao RM, Rowland KC, Spirou GA & von Gersdorff H (2002). Optimizing synaptic architecture and efficiency for high-frequency transmission. *Neuron* **36**, 1127–1143.

Thoreson WB, Rabl K, Townes-Anderson E & Heidelberger R (2004). A highly Ca^{2+}-sensitive pool of vesicles contributes to linearity at the rod photoreceptor ribbon synapse. *Neuron* **42**, 595–605.

Voets T, Neher E & Moser T (1999). Mechanisms underlying phasic and sustained secretion in chromaffin cells from mouse adrenal slices. *Neuron* **23**, 607–615.

von Gersdorff H (2001). Synaptic ribbons: versatile signal transducers. *Neuron* **29**, 7–10.

von Gersdorff H & Matthews G (1999). Electrophysiology of synaptic vesicle cycling. *Annu Rev Physiol* **61**, 725–752.

von Gersdorff H, Sakaba T, Berglund K & Tachibana M (1998). Submillisecond kinetics of glutamate release from a sensory synapse. *Neuron* **21**, 1177–1188.

von Gersdorff H, Vardi E, Matthews G & Sterling P (1996). Evidence that vesicles on the synaptic ribbon of retinal bipolar neurons can be rapidly released. *Neuron* **16**, 1221–1227.

Wangemann P & Schacht J (1996). Homeostatic mechanisms in the cochlea. In *The Cochlea*, ed. Dallos P, Popper AN, Fay RR, pp. 130–185. Springer, New York.

Wiser O, Trus M, Hernandez A, Renstrom E, Barg S, Rorsman P & Atlas D (1999). The voltage sensitive Lc-type Ca^{2+} channel is functionally coupled to the exocytotic machinery. *Proc Natl Acad Sci U S A* **96**, 248–253.

Zidanic M & Fuchs PA (1995). Kinetic analysis of barium currents in chick cochlear hair cells. *Biophys J* **68**, 1323–1336.

Acknowledgements

This work was supported by the MRC. We thank Professor W. Van der Kloot for his comments on an earlier version of the manuscript. W.M. is a Royal Society University Research Fellow.